2015

Genetically-programmed suicide of adrenergic cells in the mouse leads to severe left ventricular dysfunction, impaired weight gain, and symptoms of neurological dysfunction

Aaron Owji
University of Central Florida

GENETICALLY-PROGRAMMED SUICIDE OF ADRENERGIC CELLS IN THE MOUSE LEADS TO SEVERE LEFT VENTRICULAR DYSFUNCTION, IMPAIRED WEIGHT GAIN, AND SYMPTOMS OF NEUROLOGICAL DYSFUNCTION

by

AARON OWJI
B.S. University of Central Florida, 2012

A thesis submitted in partial fulfillment of the requirements
for the degree of Master of Science
in the Burnett School of Biomedical Sciences
in the College of Medicine
at the University of Central Florida
Orlando, Florida

Spring Term
2015

Major Professor: Steven N. Ebert

ABSTRACT

Phenylethanolamine-N-methyltransferase (Pnmt) catalyzes the conversion of noradrenaline to adrenaline and is the last enzyme in the catecholamine biosynthetic pathway. Pnmt serves as a marker for adrenergic cells, and lineage-tracing experiments have identified the embryonic heart and hindbrain region as the first sites of Pnmt expression in the mouse. Pnmt expression in the heart occurs before the adrenal glands have formed and prior to sympathetic innervation, suggesting that the heart is the first site of catecholamine production in the mouse. The function of these Pnmt+ cells in heart development remains unclear. In the present study, we test the hypothesis that (i) a genetic ablation technique utilizing a suicide reporter gene selectively destroys Pnmt cells in the mouse, and (ii) Pnmt cells are required for normal cardiovascular and neurological function.

To genetically ablate adrenergic cells, we mated Pnmt-Cre mice, in which Cre-recombinase is under the transcriptional regulation of the Pnmt promoter, and a Cre -activated diphtheria toxin A (DTA) mouse strain (ROSA26-eGFP-DTA), thereby causing activation of the toxic allele (DTA) in Pnmt-expressing (adrenergic) cells resulting in selective "suicide" of these cells in approximately half of the offspring. The other half serve as controls because they do not have the ROSA26-eGFP-DTA construct. In the $Pnmt^{+/Cre}$; $R26^{+/DTA}$ offspring, we achieve a dramatic reduction in Pnmt transcript and Pnmt immunoreactive area in the adrenal glands. Furthermore, we show that loss of Pnmt cells results in severe left ventricular dysfunction that progressively worsens with age. These mice exhibit severely reduced cardiac output and ejection fraction due to decreased LV contractility and bradycardia at rest. Surprisingly, these mice appear to have a normal stress response, as heart rate and ejection fraction increased to a similar

extent compared to controls. In addition to baseline cardiac dysfunction, these mice fail to gain body weight in a normal manner and display gross neurological dysfunction, including muscular weakness, abnormal gaiting, and altered tail suspension reflex, an indicator of neurological function.

This work demonstrates that selective Pnmt cell destruction leads to severe left ventricular dysfunction, lack of weight gain, and neurological dysfunction. This novel mouse is expected to shed insight into the role of Pnmt cells in the heart, and suggests a role for Pnmt cells in neurological regulation of feeding behavior, metabolism, and motor control.

ACKNOWLEDGMENTS

This work would not be possible without the help of certain individuals and the UCF community as a whole. I would like to thank my parents for their support and encouragement throughout my education. I am also thankful to the many professors at UCF who instilled in me the curiosity and knowledge to pursue biomedical research, both through my Bachelor's and Master's education. I would like to thank Dr. Kiminobu Sugaya for use of his cryostat and his helpful expertise in tackling new problems. I would also like to thank Dr. Stephen King for sharing his extensive expertise in mouse neuromuscular phenotyping and for the use of his Bioseb grip strength meter. I would also like to thank Dr. Mónica Moreira-Rodrigues from the University of Porto, Portugal for performing the HPLC experiments. I am also thankful to the many students and faculty who helped me overcome some of the technical challenges I encountered. Finally, I would like to thank Dr. Ebert for giving me the motivation, the training, and the tools to continue to do biomedical research.

TABLE OF CONTENTS

LIST OF FIGURES

LIST OF TABLES

LIST OF SYMBOLS AND ABBREVIATIONS

ANOVA – Analysis of Variance

BPM - Beats Per Minute

cDNA - complementary Deoxyribonucleic Acid

Cre - Cre-recombinase

Ct - Threshold Cycle

DAPI – 4’,6-Diamidino-2-Phenylindole

DNA - Deoxyribonucleic Acid

DNase - Deoxyribonuclease

DTA - Diphtheria Toxin alpha

eGFP - Enhanced Green Fluorescent Protein

g - grams

Gapdh - Glyceraldehyde 3-phosphate Dehydrogenase

HPLC – High Performance Liquid Chromatography

Ig - Immunoglobulin

IMO - Immobilization

KO – Knockout

LacZ – Beta – galactosidase gene

LV - Left Ventricle

MHz - Megahertz

mL - Milliliter

mL/min - milliliters per minute

ng - nanograms

P3.5 - Postnatal Day 3.5

PBS - Phosphate Buffered Saline

PCR - Polymerase Chain Reaction

Pnmt - Phenylethanolamine-N-methyltransferase

PSLA - Parasternal Long Axis

PVN – Paraventricular Nucleus of the Hypothalamus

R26 - Rosa26

R26R - Rosa26 Reporter

RNA - Ribonucleic Acid

RNase - Ribonuclease

ROI - Region of Interest

SV40 - Polyadenylation Sequence

μL - microliters

μm - micrometer

INTRODUCTION

Extra-Adrenal Sites of Pnmt Expression

Pheynlethanolamine-N-methyltransferase (Pnmt) performs the final catalytic step in the biosynthesis of adrenaline, methylating noradrenaline with a methyl group from the donor S-adenosylmethionine. Pnmt is primarily expressed in the adrenal glands in the adult, but many extra-adrenal sites of Pnmt expression have been identified, including the heart, brain, kidneys, and adipose tissue (Kvetnansky et al., 2012) (Spatz et al., 1982) (Ebert et al., 1996) (Ebert et al., 2008) (Ziegler et al., 1989) [for review, see – (Ziegler et al., 2002)].

Pnmt Expression in the Embryonic Heart

The first site of Pnmt expression in mouse and rat is the embryonic heart and hindbrain region (Ebert et al., 1996) (Ebert et al., 2008) (Ebert et al., 2004). In the rat, Pnmt expression begins at embryonic day 9.5 (E9.5), peaking at E10.5, and gradually decreasing until it is no longer detectable by E13.5 (Ebert et al., 1996). Pnmt+ cells were identified in close proximity to cells of the conduction system, including the sinoatrial node, atrioventricular node, His bundle, and Purkinje fibers (Ebert and Thompson, 2001) (Ebert et al., 1996). Pnmt has been identified in various cell types within the heart, including intrinsic cardiac adrenergic cells, cardiac myocytes, and intracardiac neurons (Huang et al., 1996) (Osuala et al., 2011) (Slavikova et al., 2003).

In order to study the distribution of Pnmt expression, various reporter mice have been generated (Xia et al., 2013) (Ebert et al., 2004) (Quaife et al., 1994) (Ziegler et al., 2002). Studies using fluorescent reporter under the Pnmt regulatory sequence have identified Pnmt in the atrium and ventricle of E10.5 mice and have identified Pnmt expression during differentiation of mouse

embryonic stem cells to cardiomyocytes (Xia et al., 2013). While these studies are useful to identify active Pnmt expression, they do not label historical Pnmt expression.

Pnmt Lineage Tracing

Genetic recombination strategies can be used to permanently label cells that expressed a gene of interest at some point in time. In order to identify active and historical Pnmt expression, mice expressing Cre-recombinase under transcriptional control of the Pnmt regulatory sequences (Pnmt-Cre mice) were cross-mated with Rosa26 Reporter mice, which express beta galactosidase (LacZ) in cells that express Cre-recombinase (Figure 1). Since the Cre-recombinase acts on DNA in an irreversible manner, beta galactosidase is activated in the cell permanently and is expressed in all cells derived from the original cell in which Cre-recombinase was expressed. The genetic schematic shown in Figure 1 outlines this fate-mapping approach achieved through Pnmt-Cre x Rosa26Reporter mice.

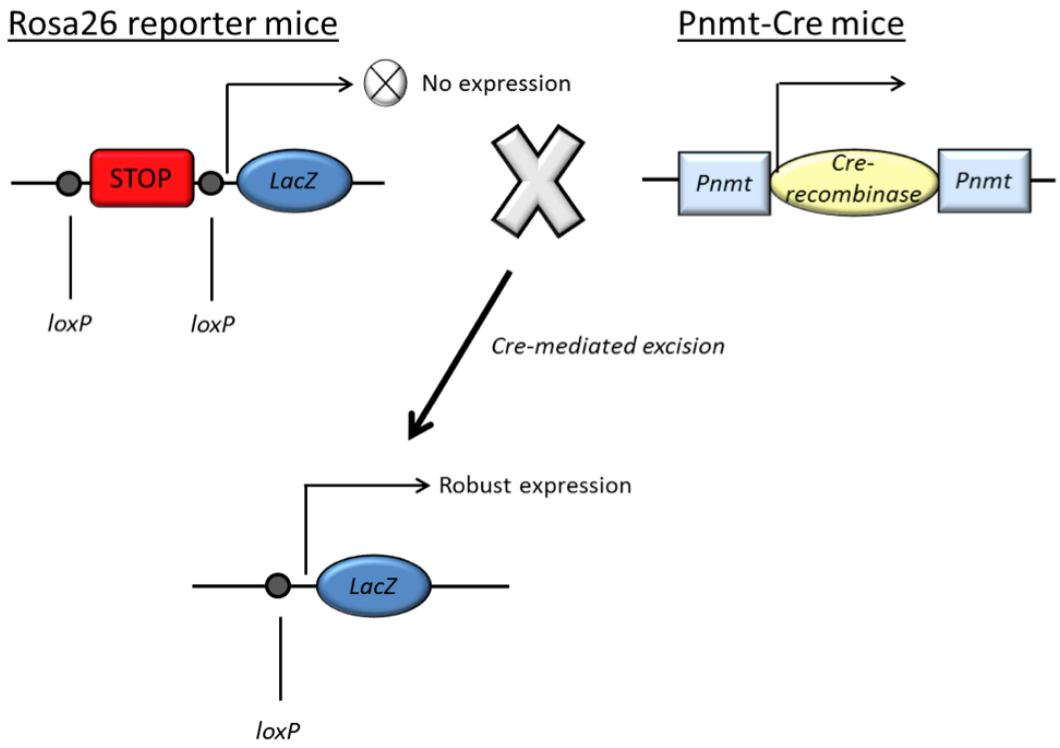

Figure 1: Overview of Genetics Schematic for Fate Mapping Experiments
Pnmt regulatory sequences drive expression of Cre-recombinase, which removes the floxed stop sequence immediately upstream of the LacZ gene. LacZ gene is expressed in all cells that expressed Pnmt at some point in time.

These fate-mapping experiments identified the heart as a major site of Pnmt expression (Ebert et al., 2004). In the embryonic whole-mount, LacZ staining was identified at E8.5 and became much more robust by E10.5, primarily labeling the myocardium, brainstem, and 2nd branchial arch (Figure 2). Between embryonic day 8.5 and 10.5, LacZ staining was identified in the sinoatrial junction of the heart, in the atrial myocardium, and in the ventricular myocardium. These results demonstrated that Pnmt+ cells and cells derived from Pnmt+ cells contribute extensively to development of myocardium and to brain stem.

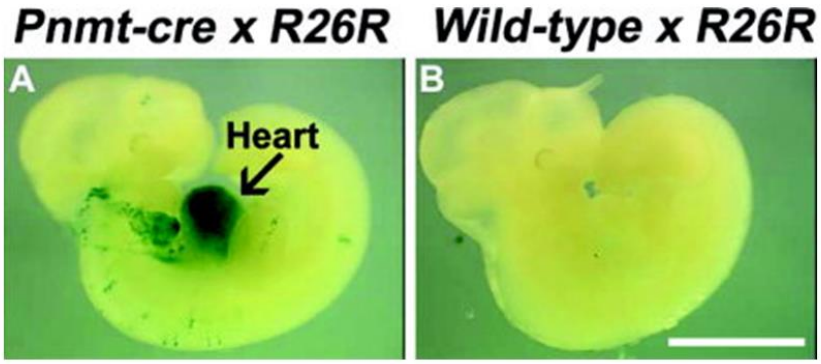

Figure 2: Fate-mapping Experiments Identified Extensive LacZ Staining in the E10.5 Mouse Heart.
A) E10.5 embryo of Pnmt-Cre/R26R, B) Control E10.5 embryo of R26R with no Pnmt-Cre. Image taken from Ebert et al., Developmental Dynamics, 2004.

Furthermore, later studies showed LacZ staining was present in the adult myocardium (Osuala et al., 2011). Specifically, historical Pnmt expression was identified in the left atrium and extensively in the free wall of the left ventricle. LacZ staining was heaviest in the left ventricle, where it was found in cardiomyocytes of the ventral regions of the apex and progressed towards the base on the dorsal side. Overall, the data provide compelling evidence for the existence of adult left ventricular myocardium that is derived from Pnmt+ cells. LacZ-stained cardiomyocytes either expressed Pnmt at some point in time or are derived from progenitors that expressed Pnmt.

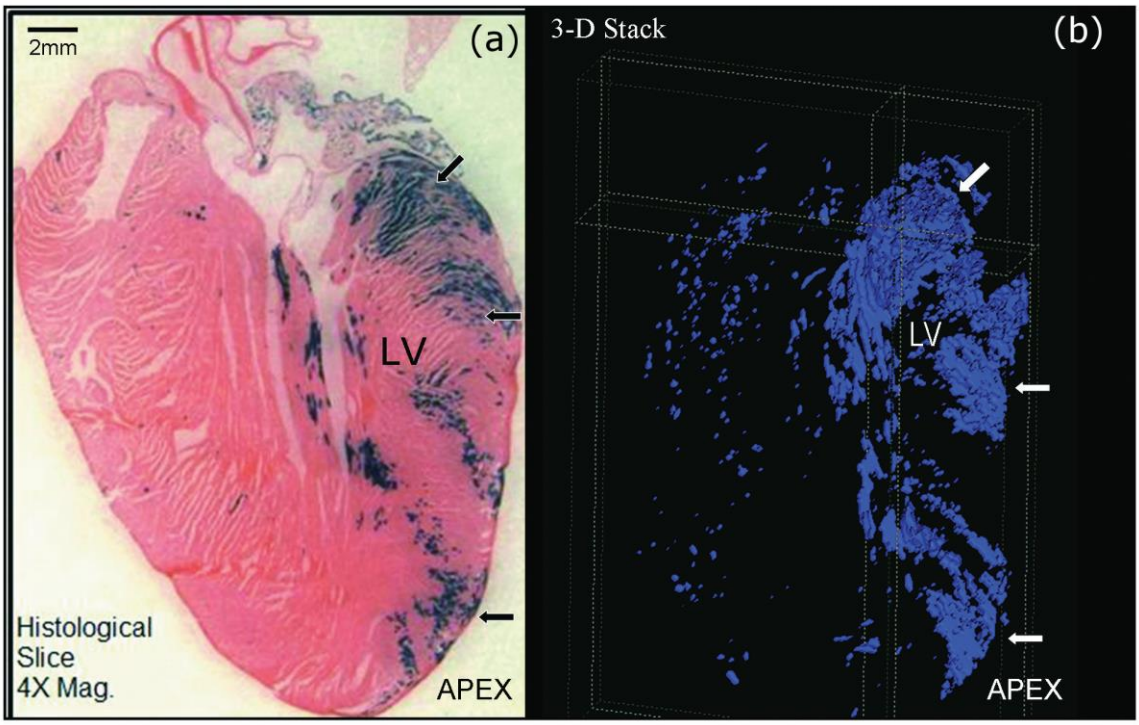

Figure 3: Lineage-Tracing Stains Historical and Active Pnmt Expression with LacZ.
(A) Pnmt lineage tracing identifies cardiomyocytes at the apex, mid, and base regions of the left ventricle. (B) 3-Dimensional reconstruction from serially stained heart indicates extensive LacZ staining throughout the LV myocardium. Figure taken from Osuala PlosONE 2011, open access.

Overview of Adrenergic Receptors

The actions of adrenaline are mediated by binding to and activating the Beta1, Beta2, and Alpha1 adrenergic receptors. Activation of the Beta1 adrenergic receptor by adrenaline increases the rate of contraction (positive chronotropism), the conductivity (positive dromotropism), and the force of contraction (positive inotropism) in the heart. Activation of Alpha1 receptors induces smooth muscle contraction and vasoconstriction, while peripheral Beta2 receptor activation results in smooth muscle relaxation and vasodilation.

The Pnmt Knockout Phenotype

Although Pnmt is extensively expressed in specific areas of the heart, adrenaline production is not necessary for basal cardiovascular function (Ebert et al., 2004). Mice

homozygous for Cre-recombinase ($Pnmt^{Cre/Cre}$) lack adrenaline and are born in normal mendelian ratios, appear normal, and exhibit no overt phenotypes to distinguish them from $Pnmt^{+/Cre}$ heterozygous controls, which do not lack adrenaline.

Another Pnmt knockout mouse has been previously described (Bao et al., 2007). This Pnmt knockout was deficient in adrenaline and exhibited normal cardiovascular physiology at rest. During exercise stress these mice became hypertensive (Bao et al., 2008) and during restraint stress all cardiovascular indices remained normal, except for a decrease in the ratio of the left ventricular posterior wall thickness to the left ventricle inner diameter during diastole, suggesting concentric remodeling (Bao et al., 2007). These mice had normal heart rate and normal blood pressure at rest.

Ablation of Pnmt+ Cells in the Mouse

Cellular ablation by genetic means is a relatively new tool in elucidation of the developmental role of specific cell populations. One previous study reported the functional effects of Pnmt+ cell destruction in mouse (Quaife et al., 1994). In the study, diphtheria toxin alpha (DTA) gene was under transcriptional control of human Pnmt regulatory sequences. Pnmt+ cell ablation resulted in smaller adrenal glands, small eyes, abnormal lens, and sterility. One major drawback of this study was that expression of the DTA transgene was not under normal mouse transcriptional regulation. Rather, 2kb of human Pnmt 5' upstream region was ligated to the DTA gene and randomly integrated into mouse oocyte. The effects on cardiovascular system and behavior were not reported. Furthermore, the DTA gene was under regulatory control of human Pnmt, rather than mouse Pnmt, so DTA gene expression may not faithfully recapitulate normal Pnmt expression in the mouse.

In order to identify the functional role of Pnmt-expressing cells in the heart, we have utilized a novel cell suicide model to ablate Pnmt+ cells in the developing mouse. Instead of crossing $Pnmt^{Cre/Cre}$ mice with R26R Beta Galactosidase reporter mice, they were crossed with ROSA26-eGFP-DTA mice. These mice express the diphtheria toxin alpha (DTA) subunit upon activation of Cre-recombinase (Ivanova et al., 2005). This is expected to provide selective and sensitive ablation of Pnmt+ cells throughout the entire mouse, including the heart. Diphtheria toxin alpha induces cell death through ADP ribosylation of elongation factor 2, leading to inhibition of protein synthesis (Collier, 2001) (Evans, 1989). Ivanova et al have estimated that cells die within 24 hours of endogenous expression of DTA. This system is devised to better recapitulate normal mouse Pnmt expression. Since Cre-recombinase is knocked-in to exon1 of the mouse Pnmt gene, it is under normal transcriptional control.

The goals of the present study are to test the hypothesis that: (i) breeding $Pnmt^{Cre/Cre}$ mice with ROSA26-eGFP-DTA mice produces selective destruction of Pnmt+ cells and (ii) selective destruction of Pnmt+ cells results in cardiovascular dysfunction.

MATERIALS AND METHODS

Mice

All procedures and handling of mice were conducted in accordance with the University of Central Florida Institutional Animal Care and Use Committees. The $Pnmt^{Cre/Cre}$ and Rosa26-eGFP-DTA mice have been described previously (Ebert et al., 2004) (Ivanova et al., 2005). $Pnmt^{Cre/Cre}$ mice were maintained in homozygous conditions, while Rosa26-eGFP-DTA mice were bred to generate $R26^{+/DTA}$ females. For all experiments described here, $Pnmt^{Cre/Cre}$ males were bred with $R26^{+/DTA}$ females to produce offspring that were either $Pnmt^{+/Cre}$; $R26^{+/+}$ or $Pnmt^{+/Cre}$; $R26^{+/DTA}$. Mice were genotyped using primers previously described by Ivanova et al (2008). Pure DNA was isolated from tail snips taken at the time of weaning and PCR was performed using the following primers: R26R1 5'-AAAGTCGCTCTGAGTTGTTAT-3', R26R2 5'-GCGAAGAGTTTGTCCTCAACC-3', and R26R3 5'-GGAGCGGGAGAAATGGATATG-3'.

Echocardiography

Transthoracic echocardiography was performed with the VisualSonics Vevo2100 equipped with an MS550 transducer (40MHz) for cardiovascular imaging. Adult mice were lightly anesthetized with 1.5-2.0% isoflurane to minimize reductions in heart rate. Analysis was performed on parasternal long axis (PSLA) M mode images of the left ventricle (LV) using Vevo2100 software v 1.6.0. For all baseline measurements, heart rate was obtained by the Vevo ECG board. For immobilization echocardiography, mice were first anesthetized, and baseline recordings taken. Mice were then immobilized on a heated surface in the absence of anesthesia and allowed to regain consciousness. PSLA recordings of the LV were taken at 1 hour and 2

hours after the mouse regained consciousness. For heart rate measurements during restraint, mice were taped to a pre-warmed tray at 37 degrees Celsius, so ECG could not be obtained with the Vevo system. Instead, the heart rate trace function of the Vevo software was used to calculate the heart rate from 8-10 consecutive cardiac cycles. For ultrasound analysis, two independent observers blinded to genotype performed LV tracing using the Vevo2100 software version 1.6.0. LV trace measurements were performed on four consecutive cardiac cycles, preferably between respiratory inspirations to avoid artifacts produced by abdominal cavity movements.

Gene Expression

Fresh tissue was flash-frozen in liquid nitrogen and stored at -80 degrees Celsius. RNA was isolated from flash-frozen adrenal glands using 1 mL TRIzol reagent. Genomic DNA was removed by treatment with RNase-free DNase (Promega), recovered by phenol-chloroform extraction, and genomic DNA contamination was determined by PCR using primers for the housekeeping gene Gapdh. 400 ng of pure RNA was converted to cDNA using High Capacity cDNA Reverse Transcription Kit (Invitrogen). Real-time PCR was performed using SYBR Green Fast reagent in an ABI7500 machine (Applied Biosystems) in 25 uL reactions. Genes of interest were normalized to the housekeeping gene Glyceraldehyde-3-phosphate Dehydrogenase (Gapdh). Forward and reverse primers for Pnmt have been described previously and were as follows: forward 5'-GGTGGCTCAGACCTGAAG-3' and reverse 5'-GCCATCAGGGTTGCTCAG-3'(Xia et al., 2013). Forward and reverse primers for Gapdh were as follows: forward 5'-AGAGATGATGACCCTTTGGC-3' and reverse 5'-CCATCACCATCTTCCAGGAGCG-3'. The product was detected on a 2% agarose gel to verify the product size, which was 149 base pairs for Gapdh and 183 base pairs for Pnmt. Relative

Pnmt gene expression was calculated by delta delta Ct method using Gapdh as endogenous control and normalized to $Pnmt^{+/Cre}$; $R26^{+/+}$ littermates (Schmittgen and Livak, 2008).

Histology

All tissue was fixed overnight in 4% paraformaldehyde at 4 degrees C, washed 3x10 minutes in PBS at room temperature, and then immersed in 30% sucrose in PBS at 4 degrees C. Tissue was kept in 30% sucrose for at least 2 days to allow it to sink, embedded in optimal cutting temperature solution, and then cryosectioned. Slides were either stained immediately or kept at -20 degrees Celsius until staining.

Adrenal Gland Immunofluorescence

Adult adrenal glands were processed as described and then cryosectioned at 12 micrometers and stored at -20 degrees C until stained. Slides were stained with antibody as previously described. Sections were allowed to dry at room temperature, circled with a hydrophobic barrier pen, rehydrated in PBS for 20 minutes at room temperature, blocked in blocking solution (5% w/v dry nonfat milk, 0.3% v/v Triton X-100, 0.02% sodium azide, in PBS) for 30 minutes at room temperature. Primary rabbit anti-Pnmt antibody (polyclonal rabbit anti-Pnmt from Sigma – product SAB2701157) was added to fresh blocking solution (1:100 dilution) and sections were incubated for 1 hour at room temperature and then 12-16 hours at 4 degrees Celsius in a humidified chamber. After incubation with the primary antibody, sections were washed 3x10 min in PBS at room temperature. Secondary antibody (polyclonal goat anti-Rabbit IgG – AlexaFluor 647 from Molecular Probes product A-21245) was incubated in blocking solution (1:200 dilution) for 2 hours at room temperature in a dark humidified chamber. DAPI was included in the secondary antibody solution. Sections were washed 3x10 minutes in

PBS at room temperature then mounted in FluoroGel aqueous mounting medium (Electron Microscopy Sciences). After slides hardened at room temperature, they were imaged.

All sections were imaged in the same manner on a Zeiss 710 confocal microscope using a Plan-Apochromat 20x/0.8 M27 objective. Image acquisition settings for the DAPI, eGPF, and Pnmt channels can be found in Table 1.

Table 1: Confocal Microscope Acquisition Settings for Pnmt Threshold Imaging

	DAPI	eGFP	Pnmt
Laser (nm) and power (%)	405 (2.0%)	488 (2.0%)	633 (4.0%)
Master Gain	550	750	800
Emission Filter	410-469	493-549	650-740
Pinhole (μm)	27	31	41
Beam Splitter	MBS -405	MBS 488/543/633	MBS 488/543/633

% Adrenal Gland Area Expressing Threshold Level of Pnmt

The entire adrenal medulla was sectioned and the two median medullary sections were stained. The Pnmt channel of 20X images of adrenal glands was processed in ImageJ (Schneider et al., 2012). RGB stacks were converted to 8-bit images, inverted, and the same threshold was set to each image. The threshold was set as the highest value that reduced background noise in the adrenal cortex without compromising signal from the adrenal medulla (highest signal to noise ratio). The percent area expressing a threshold level of Pnmt was calculated by creating a ROI and measuring the percent of ROI area that met threshold fluorescence in each adrenal medulla. The average of 20 ROI's were taken for each section and the two median medullary sections were averaged to give the value for one adrenal gland.

Quantitation of Catecholamines by HPLC

Adult adrenal glands were snap-frozen in 300 uL of 0.2 M perchloric acid and shipped to our collaborators in Porto, Portugal, where they underwent alumina oxide extraction and subsequent HPLC with electrochemical detection. Detailed methods for the quantitation of adrenaline and noradrenaline in adrenal glands have been previously described (Moreira-Rodrigues et al., 2014).

Grip Strength Measurements

Mice underwent grip-strength testing at 6 months. Grip-strength test was performed in a consistent manner by trained personnel on a BIO-GS3 grip strength testing device (Bioseb). First, strength in forelimbs was recorded on four consecutive trials, followed by four consecutive trials of all limbs. The average of all four trials was used to represent each mouse. Grip strength was normalized to mouse body mass to account for the weight differences between groups.

Statistical Analysis

Statistical analysis of results between two groups was performed using student's T-test or analysis of variance (ANOVA), where appropriate. ANOVA was performed by Graphpad Prism software using the Bonferroni correction for multiple comparisons. P-value less than 0.05 was required to reject the null hypothesis. Data are presented as the mean ± standard error.

RESULTS

Generation of Pnmt$^{+/Cre}$; R26$^{+/DTA}$ Mice

The generation of Pnmt-Cre mice has been previously described. These mice have Cre-recombinase inserted into the starting region of exon 1, as shown in Figure 4A. Cre-recombinase is followed by a stop sequence; therefore, Cre-recombinase is under transcriptional control of the Pnmt promoter region and Pnmt is not expressed from this site. Mice homozygous for Cre-recombinase, denoted Pnmt$^{Cre/Cre}$, do not express the adrenaline biosynthetic enzyme Pnmt and lack adrenaline. Mice heterozygous for Cre-recombinase, denoted Pnmt$^{+/Cre}$, have one wild type allele and express Pnmt at this wild type allele and Cre-recombinase from the other allele. The Rosa26-eGFP-DTA mice were purchased from the Jackson Laboratory (product #006331). These mice have been previously described and are used to ablate cells in a Cre-dependent manner (Ivanova et al., 2005).

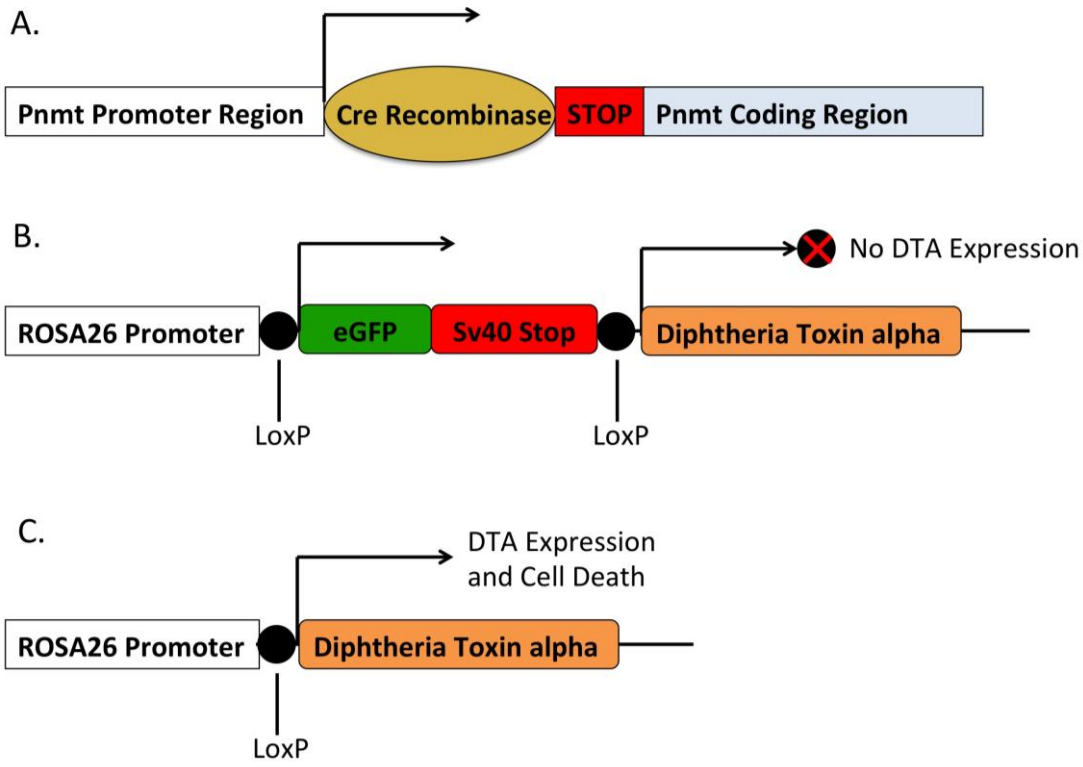

Figure 4: Schematic of Genetic Constructs
A) Pnmt-Cre construct, B), ROSA26-eGFP-DTA construct, and C) Product of Cre-recombinase at Rosa26 locus in ROSA26-eGFP-DTA mice. Cre-mediated recombination at LoxP sites of the Rosa26 locus results in removal of the upstream triple SV40 polyadenylation sequence and of eGFP. Consequently, Cre-recombinase activity in Pnmt+ cells results in loss of eGFP expression and activation of DTA expression.

As shown in Figure 4B, which depicts the Rosa26-eGFP-DTA construct prior to the introduction of Cre-recombinase, the Diphtheria Toxin alpha gene (DTA) is preceded by a floxed eGFP and triple SV40 polyadenylation sequence, a strong transcriptional terminator. eGFP is expressed constitutively in all cells in the absence of Cre-recombinase and the DTA gene is not transcribed due to the upstream SV40 polyadenylation sequence. Figure 4C depicts the Rosa26 locus following Cre-recombinase activity, in which the floxed eGFP and SV40 sequence have been removed, resulting in loss of eGFP expression and activation of DTA expression.

To generate Pnmt$^{+/Cre}$; R26$^{+/DTA}$ mice, Pnmt$^{Cre/Cre}$ males were bred with R26$^{+/DTA}$ females. This cross is expected to generate 50% Pnmt$^{+/Cre}$; R26$^{+/DTA}$ mice (ablation groups) and 50% Pnmt$^{+/Cre}$; R26$^{+/+}$ mice (control group), or 25% male and 25% female for each genotype. Table 2 depicts the observed frequency of mice that lived to age of weaning (approximately 21 days). The expected frequency of males and females in each group is 25%, yet the observed frequency of Pnmt$^{+/Cre}$; R26$^{+/DTA}$ females was 15.4%. Chi squared analysis was performed to test whether these observed ratios deviated significantly from the expected ratios (25% of each sex in each group). It was found that there was a sex-linked deviation from expected mendelian ratios. That is, among the Pnmt$^{+/Cre}$; R26$^{+/DTA}$ group, there were 47 males and 23 females and this deviation from expected values was found to be statistically significant with p value = 0.0028. There was no statistically significant deviation from expected values within the control Pnmt$^{+/Cre}$; R26$^{+/+}$ group (p=0.2499). The relative percent of each genotype by sex is displayed in Table 2.

Table 2: Frequency of Viable Pups at Weaning From Pnmt$^{Cre/Cre}$ x R26$^{+/DTA}$ Matings.
The two possible genotypes are listed with the number of viable pups for each sex at age of weaning. Only Pnmt$^{+/Cre}$; R26$^{+/DTA}$ females deviated greatly from the expected 25%. This discrepancy was found to be statistically significant by Chi squared distribution test (**p=0.0028) for Male v Female amongst Pnmt$^{+/Cre}$; R26$^{+/DTA}$ offspring.

	Male	Female
Pnmt$^{+/Cre}$; R26$^{+/+}$	28.9% (43/149)	24.2% (36/149)
Pnmt$^{+/Cre}$; R26$^{+/DTA}$	31.5% (47/149)	15.4% (23/149)**

Characterization of Adrenal Gland Contents of Pnmt$^{+/Cre}$; R26$^{+/DTA}$ Mice

Pnmt Gene Expression in Pnmt$^{+/Cre}$; R26$^{+/DTA}$ Mice

The results of Pnmt gene expression analysis in 6-month-old adrenal glands are depicted in Figure 5. Pnmt mRNA levels were 97.6% lower in the adrenal glands of Pnmt$^{+/Cre}$; R26$^{+/DTA}$

mice compared to those of Pnmt$^{+/Cre}$; R26$^{+/+}$ mice. Furthermore, Pnmt mRNA levels were 37.9% higher in the adrenal glands of R26$^{+/DTA}$ mice compared to those of Pnmt$^{+/Cre}$; R26$^{+/+}$, but the difference was not statistically significant (p=0.119). Pnmt$^{+/Cre}$; R26$^{+/+}$ mice have one wild-type allele for Pnmt and their catecholamine concentrations have been previously reported and did not differ from wild-type mice (Ebert et al., 2004).

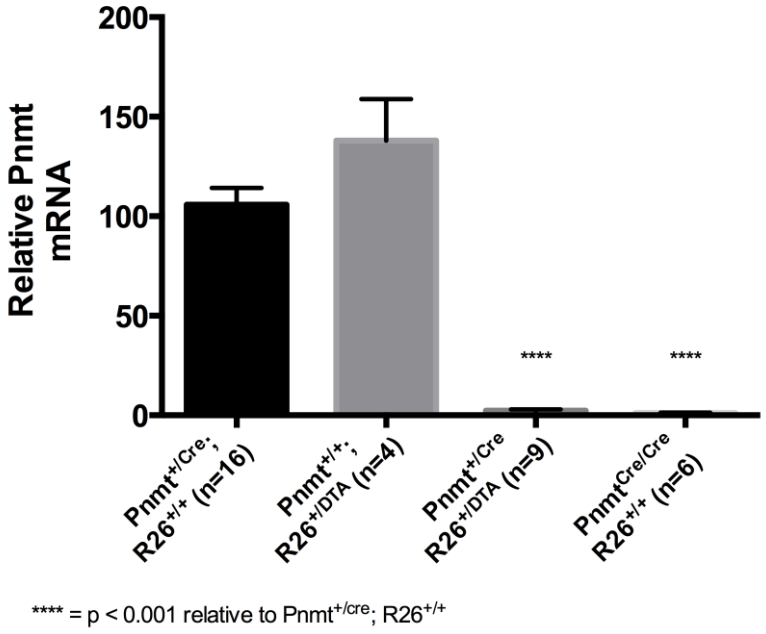

Figure 5: RT-PCR Analysis of Pnmt mRNA Expression in Mouse Adrenal Glands

Quantitation of Pnmt+ Area by Immunofluorescent Staining

Using immunofluorescent staining techniques, Pnmt+ cells were identified in the adrenal medulla of Pnmt$^{+/Cre}$; R26$^{+/+}$ and Pnmt$^{+/Cre}$; R26$^{+/DTA}$ mice at P3.5. A typical Pnmt$^{+/Cre}$; R26$^{+/+}$ control adrenal gland for postnatal day 3 pup is shown in Figure 6A, with a closeup in Figure 6E, and a typical Pnmt$^{+/Cre}$; R26$^{+/DTA}$ adrenal gland is shown in Figure 6B, with a closeup in Figure 6F. Pnmt+ cells were also identified at 6 months of age in Pnmt$^{+/Cre}$; R26$^{+/+}$ and Pnmt$^{+/Cre}$; R26$^{+/DTA}$. A 6 month old Pnmt$^{+/Cre}$; R26$^{+/+}$ adrenal gland is shown in Figure 6C, with a closeup in

Figure 6G, and a 6 month old Pnmt$^{+/Cre}$; R26$^{+/DTA}$ adrenal gland is shown in Figure 6D, with a closeup in Figure 6H. Pnmt is colored red and the nuclei were stained with DAPI, shown in blue.

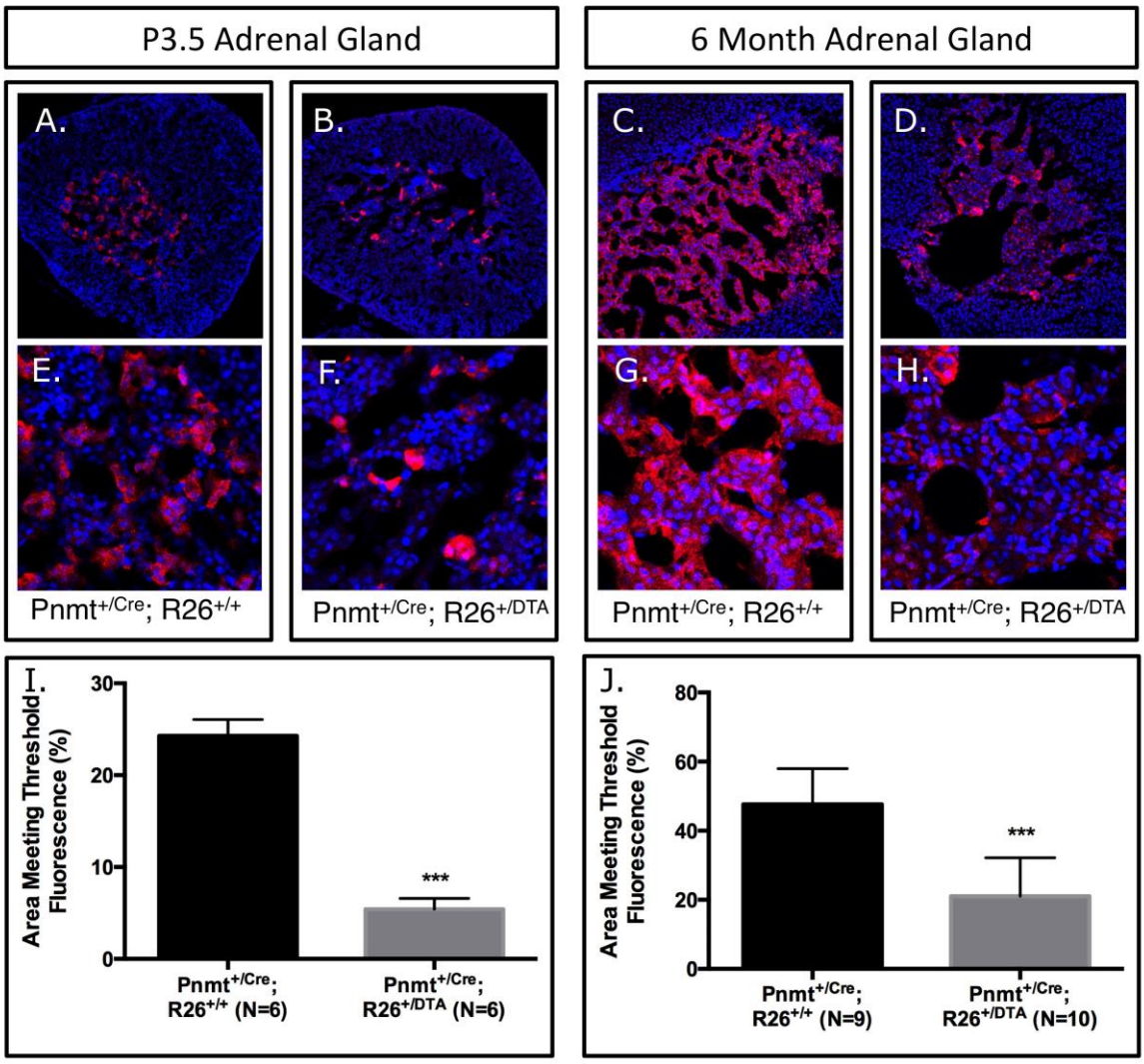

Figure 6: Immunofluorescent Analysis of Pnmt+ Area in Early Postnatal and Adult Adrenal Glands
Pnmt immunofluorescence in P3.5 (A, B, closeups in E, F) and 6 month adrenal glands (C, D, clcoseups in G, H) in Pnmt$^{+/Cre}$; R26$^{+/+}$ and Pnmt$^{+/Cre}$; R26$^{+/DTA}$. (I) Decreased % area meeting threshold fluorescence within the adrenal gland at P3.5. (J) Decreased % area meeting threshold fluorescence in adrenal gland at 6 months.

The relative area of adrenal medulla expressing Pnmt protein was markedly reduced in P3.5 and 6-month-old adrenal glands of Pnmt$^{+/Cre}$; R26$^{+/DTA}$ mice. At postnatal day 3.5, the

percent of medulla area expressing Pnmt was decreased by 77.7% compared to controls (5.42±1.17, n=6 v 24.28±1.78, n=6, $p<0.0001$), as shown in Figure 6I. At 6 months, the percent of medulla area expressing Pnmt was decreased by 55.8% compared to controls (21.02±3.519, n=10 v 47.61±3.462, n=9, $p<0.0001$), as shown in Figure 6J.

Pnmt+, eGFP- cells were identified in 6-month-old adrenal glands in the $Pnmt^{+/Cre}$; $R26^{+/DTA}$ mice. The white arrows of Figure 7D denote Pnmt+ cells in red and Figure 7C shows that these same cells do not express eGFP. The Pnmt+, eGFP- cells also express tyrosine hydroxylase (TH), depicted in white in Figure 7B. As shown in the overlay, Figure 7E, Pnmt+, TH+, eGFP- cells are surrounded by Pnmt-, TH-, eGFP+ cells in the adrenal gland. These Pnmt+, TH+, eGFP- cells are likely at a timepoint after Cre-mediated recombination removed the floxed eGFP and upstream SV40 polyadenylation sequence at the Rosa26 locus and are expected to undergo apoptosis due to activation of DTA expression.

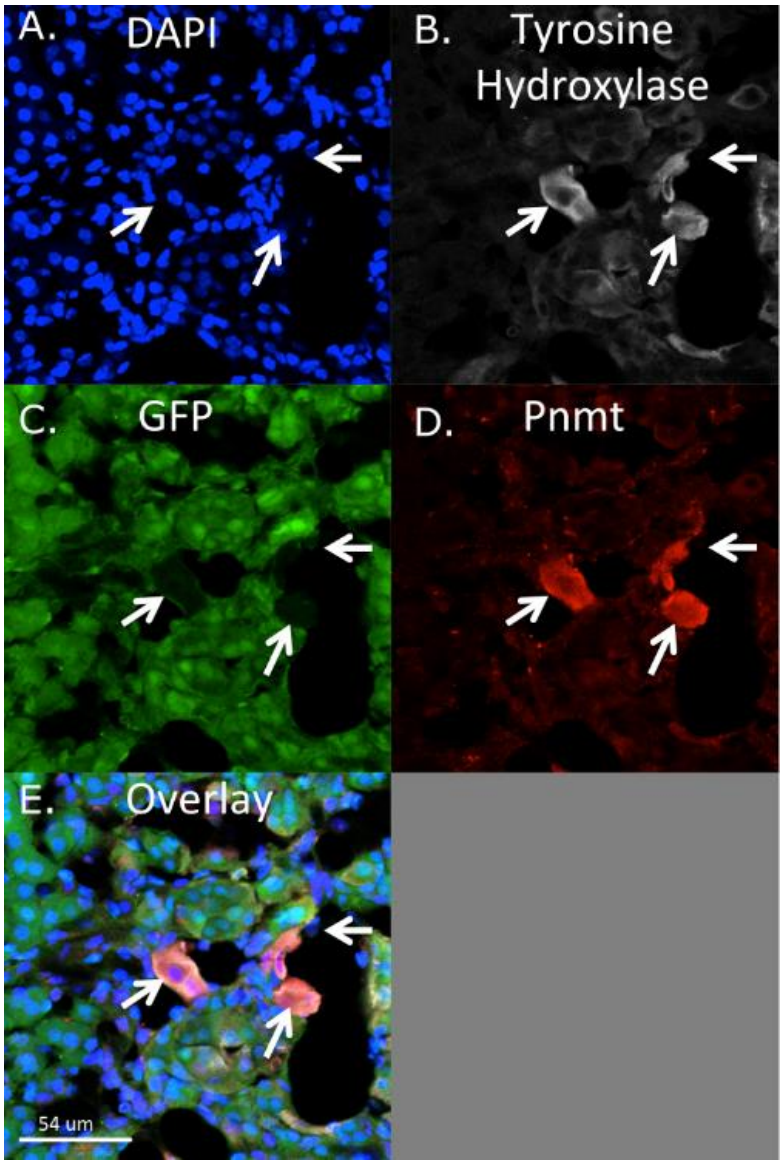

Figure 7: GFP is Not Expressed in Pnmt+ Cells, but is Expressed in Surrounding Pnmt- Cells
(A) DAPI labels nuclei in blue. (B) Tyrosine Hydroxylase (TH) in white. (C) GFP in green. (D) Pnmt in red. (E) Overlay of all channels. White arrows point to three Pnmt+, TH+, GFP- cells.

Quantitation of Catecholamine Contents in Pnmt$^{+/Cre}$; R26$^{+/DTA}$ Mice

Whole adult adrenal glands were homogenized in perchloric acid. Catecholamines were extracted by alumina oxide and separated by HPLC, followed by electrochemical detection. The

total adrenaline content is depicted in Figure 8A and the total noradrenaline content is depicted in Figure 8B.

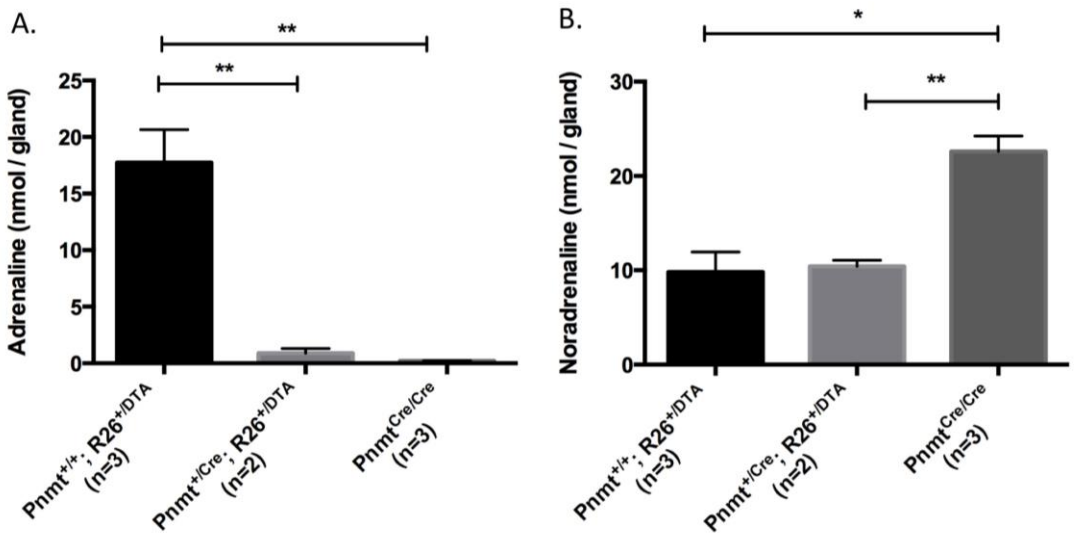

Figure 8: HPLC for Adrenaline and Noradrenaline content of Adult Adrenal Glands
(A) Total adrenaline in adult adrenal glands. (B) Total noradrenaline in adult adrenal glands.

Adrenaline is significantly reduced in $Pnmt^{+/Cre}$; $R26^{+/DTA}$ and Pnmt KO adrenals. The adrenaline levels did not differ significantly between the $Pnmt^{+/Cre}$; $R26^{+/DTA}$ group and Pnmt knockout group. Both groups had significantly lower adrenaline content than the $Pnmt^{+/+}$; $R26^{+/DTA}$ control group. The $Pnmt^{+/Cre}$; $R26^{+/DTA}$ adrenal gland had comparable levels of noradrenaline to $Pnmt^{+/+}$; $R26^{+/DTA}$ adrenals. The Pnmt knockout adrenals had significantly more noradrenaline than both groups, which is expected and in agreement with previous reports due to build-up of noradrenaline in cells that would normally be adrenergic (Ebert et al., 2004; Moreira-Rodrigues et al., 2014). These results suggest that $Pnmt^{+/Cre}$; $R26^{+/DTA}$ adrenal glands lack Pnmt+ cells that produce adrenaline, because the adrenaline content was comparable to knockouts. In contrast with Pnmt knockout adrenal glands, $Pnmt^{+/Cre}$; $R26^{+/DTA}$ adrenals do not build up

noradrenaline. Pnmt knockout effectively converts adrenergic cells to a noradrenergic phenotype and noradrenaline builds up in these cells. In the $Pnmt^{+/Cre}$; $R26^{+/DTA}$ mouse, adrenergic cells are killed, resulting in adrenaline levels comparable to knockout levels, but noradrenaline levels remain physiological.

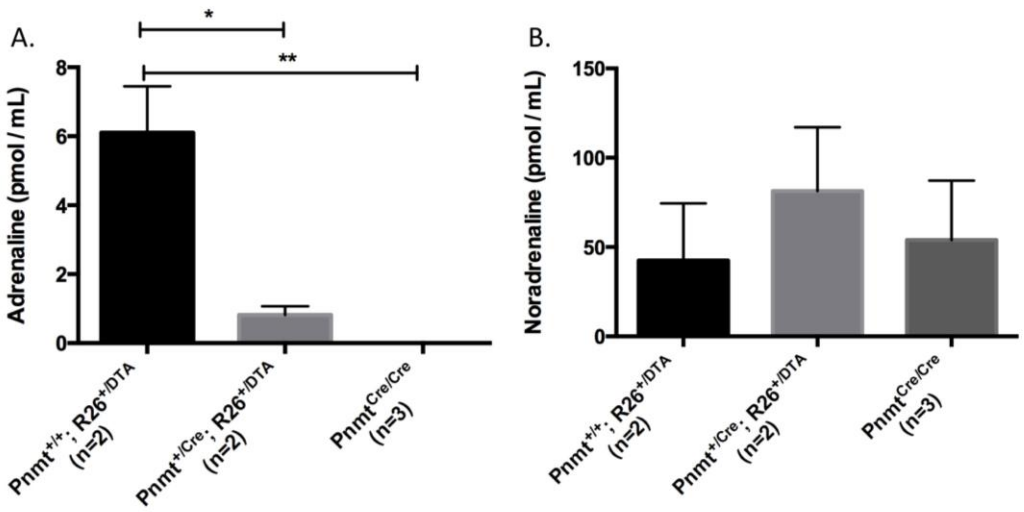

Figure 9: HPLC for Adrenaline and Noradrenaline in Adult Plasma
(A) HPLC for adrenaline in $Pnmt^{+/Cre}$; $R26^{+/+}$, $Pnmt^{+/Cre}$; $R26^{+/DTA}$, and $Pnmt^{Cre/Cre}$ (Pnmt KO) adrenal glands. $Pnmt^{Cre/Cre}$ was below the limit of detection and represented as baseline. (B) HPLC for noradrenaline in all three mouse genotypes. No significant differences.

Figure 9A depicts the levels of adrenaline in adult mouse plasma in the three groups tested. Adrenaline in the Pnmt KO was baseline. Adrenaline was significantly lower in the $Pnmt^{+/Cre}$; $R26^{+/DTA}$ group and the Pnmt KO group. Adrenaline was not significantly different between the $Pnmt^{+/Cre}$; $R26^{+/DTA}$ group and Pnmt KO group. Noradrenaline was not significantly different between any of the groups, as shown in Figure 9B. Because noradrenaline was significantly higher in the adrenal glands of the Pnmt KO group, but not in the plasma of these mice, it is possible that circulating noradrenaline levels only drastically increase in response to certain stimuli, such as stress, but this is unclear at this time.

Taken together, these data provide support for the hypothesis that crossing $Pnmt^{Cre/Cre}$ males with $R26^{+/DTA}$ females produces $Pnmt^{+/Cre}$; $R26^{+/DTA}$ mice that have severely reduced number of Pnmt+ cells in the adrenal gland. These mice had significantly reduced Pnmt transcript, decreased number of Pnmt+ cells in the adrenal medulla, and had significantly reduced adrenaline stored in their adrenal glands and in circulation. Furthermore, the identification of Pnmt+, eGFP- cells surrounded by Pnmt-, eGFP+ cells in the adrenal medulla suggests that the genetic construct is working, since eGFP was not expressed in Pnmt+ cells.

Cardiovascular Phenotype of $Pnmt^{+/Cre}$; $R26^{+/DTA}$ Mice

$Pnmt^{+/Cre}$; $R26^{+/DTA}$ Mice Have Diminished LV Function

To test the functional effects Pnmt+ cell ablation, echocardiography of $Pnmt^{+/Cre}$; $R26^{+/DTA}$ mice was performed on a monthly basis for 6 months. $Pnmt^{+/Cre}$; $R26^{+/DTA}$ mice exhibited bradycardia at all timepoints, as depicted in Figure 10A.

Furthermore, ejection fraction, stroke volume, and cardiac output were significantly reduced at all timepoints, as shown in Figures 10B, 10C, and 10D, respectively. These data are summarized in Table 3.

Table 3: Summary of Monthly Echocardiographic Data

	1 Month			2 Month			3 Month		
	$Pnmt^{+/Cre}$; $R26^{+/+}$	$Pnmt^{+/Cre}$; $R26^{+/DTA}$		$Pnmt^{+/Cre}$; $R26^{+/+}$	$Pnmt^{+/Cre}$; $R26^{+/DTA}$		$Pnmt^{+/Cre}$; $R26^{+/+}$	$Pnmt^{+/Cre}$; $R26^{+/DTA}$	
	N=26	N=24	p-value	N=11	N=7	p-value	N=15	N=10	p-value
Heart Rate (BPM)	428 ± 8	400 ± 8	0.019	440 ± 11	412 ± 7	0.085	442 ± 10	383 ± 7	<0.001
Stroke Volume (μL)	35 ± 1	31 ± 1	0.04	35 ± 2	28 ± 3	0.035	39 ± 2	25 ± 2	<0.001
Ejection Fraction (%)	67 ± 2	57 ± 2	<0.001	64 ± 3	51 ± 5	0.033	60 ± 3	49 ± 3	0.029
Fractional Shortening (%)	37 ± 1	30 ± 1	<0.001	35 ± 2	26 ± 4	0.054	32 ± 2	24 ± 2	0.022
Cardiac Output (mL/min)	15 ± 1	13 ± 1	0.006	16 ± 1	12 ± 1	0.011	17 ± 1	10 ± 1	<0.001
Systolic Diameter (μm)	2.3 ± 0.1	2.6 ± 0.1	0.007	2.4 ± 0.1	2.7 ± 0.2	0.209	2.7 ± 0.1	2.7 ± 0.2	0.967
Diastolic Diameter (μm)	3.6 ± 0.1	3.6 ± 0.1	0.431	3.6 ± 0.1	3.6 ± 0.2	0.985	3.9 ± 0.1	3.5 ± 0.2	0.042
	4 Month			5 Month			6 Month		
	$Pnmt^{+/Cre}$; $R26^{+/+}$	$Pnmt^{+/Cre}$; $R26^{+/DTA}$		$Pnmt^{+/Cre}$; $R26^{+/+}$	$Pnmt^{+/Cre}$; $R26^{+/DTA}$		$Pnmt^{+/Cre}$; $R26^{+/+}$	$Pnmt^{+/Cre}$; $R26^{+/DTA}$	
	N=18	N=14	p-value	N=17	N=12	p-value	N=18	N=12	p-value
Heart Rate (BPM)	447 ± 9	387 ± 9	<0.001	452 ± 8	410 ± 13	0.005	477 ± 11	388 ± 15	<0.001
Stroke Volume (μL)	41 ± 1	27 ± 2	<0.001	43 ± 1	30 ± 1	<0.001	42 ± 2	29 ± 2	<0.001
Ejection Fraction (%)	63 ± 2	51 ± 2	0.001	66 ± 2	52 ± 3	<0.001	66 ± 2	53 ± 5	<0.001
Fractional Shortening (%)	34 ± 2	26 ± 1	0.002	36 ± 2	27 ± 2	<0.001	36 ± 1	28 ± 3	0.013
Cardiac Output (mL/min)	18 ± 1	11 ± 1	<0.001	19 ± 1	12 ± 1	<0.001	20 ± 1	11 ± 1	<0.001
Systolic Diameter (μm)	2.6 ± 0.1	2.6 ± 0.1	0.738	2.5 ± 0.1	2.7 ± 0.1	0.114	2.4 ± 0.1	2.6 ± 0.1	0.278
Diastolic Diameter (μm)	3.9 ± 0.1	3.5 ± 0.1	<0.001	3.9 ± 0.1	3.7 ± 0.1	0.090	3.8 ± 0.1	3.6 ± 0.1	0.125

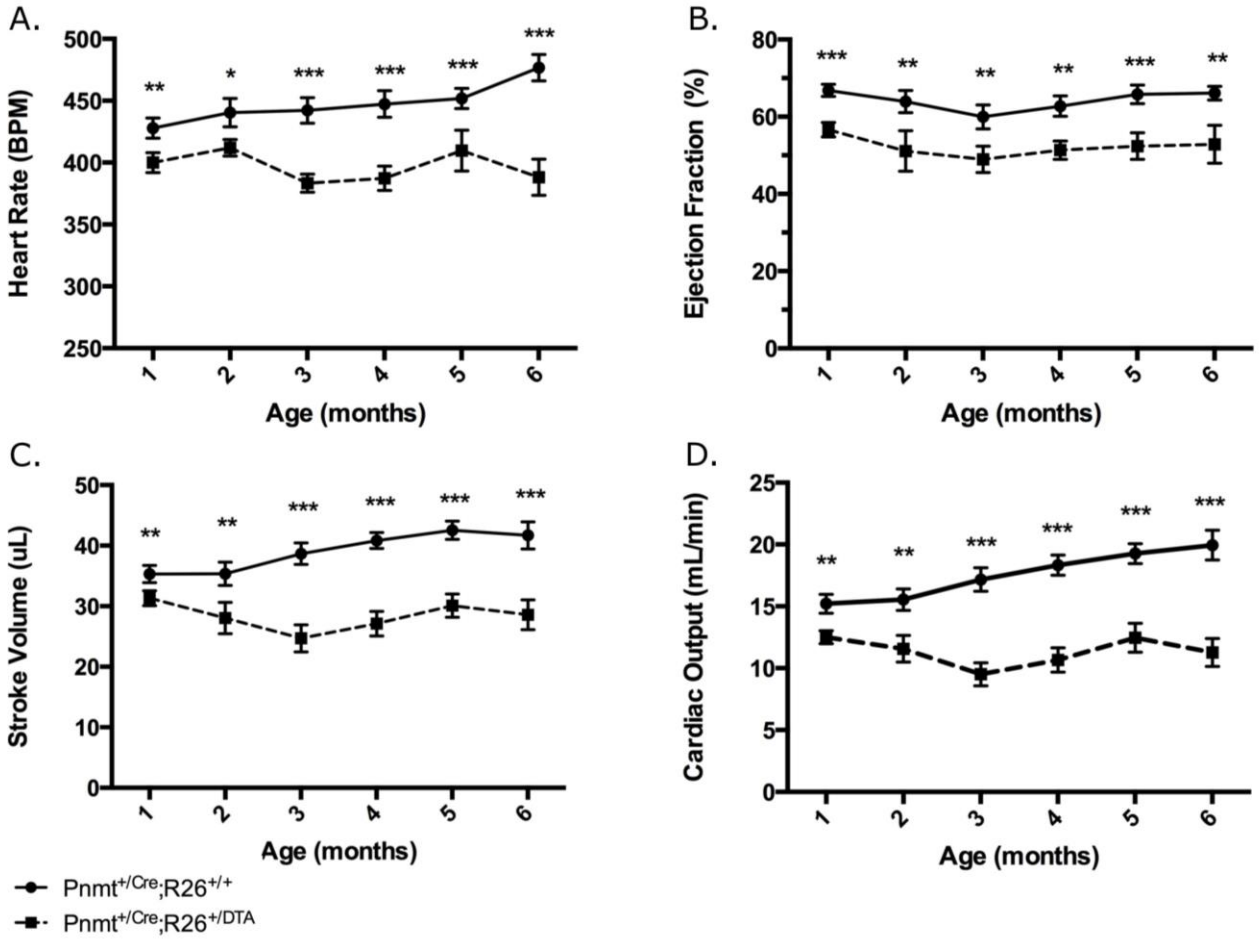

Figure 10: Echocardiography Reveals Left Ventricular Dysfunction in Pnmt$^{+/Cre}$; R26$^{+/DTA}$ Mice
(A) Heart rate was decreased in Pnmt$^{+/Cre}$; R26$^{+/DTA}$ compared to Pnmt$^{+/Cre}$; R26$^{+/+}$ at all timepoints. (B) Ejection fraction was lower at all timeptoints. (C) Stroke volume was lower at all timepoints. (D) Cardiac output, the product of heart rate and stroke volume, was lower at all timepoints.

To test whether the decrease in left ventricular function was due to loss of Pnmt+ cells or to the loss of circulating adrenaline, Pnmt KO mice underwent echocardiography at 5 months of age. Pnmt KO mice lack adrenaline and their LV function did not differ from Pnmt$^{+/Cre}$; R26$^{+/+}$ mice. This is consistent with another report of Pnmt KO mice (Bao et al., 2007). Pnmt$^{+/Cre}$; R26$^{+/DTA}$ mice had significantly diminished LV function compared to Pnmt KO mice. Ejection

fraction, stroke volume, and cardiac output were significantly decreased in the Pnmt$^{+/Cre}$; R26$^{+/DTA}$ group compared to the Pnmt KO group at 5 months of age, as shown in Figures 11B, 11C, and 11D. Heart rate was not significantly decreased in the Pnmt$^{+/Cre}$; R26$^{+/DTA}$ group compared to Pnmt KO. Table 4 summarizes the echocardiographic data of these 3 types of mice at 5 months of age.

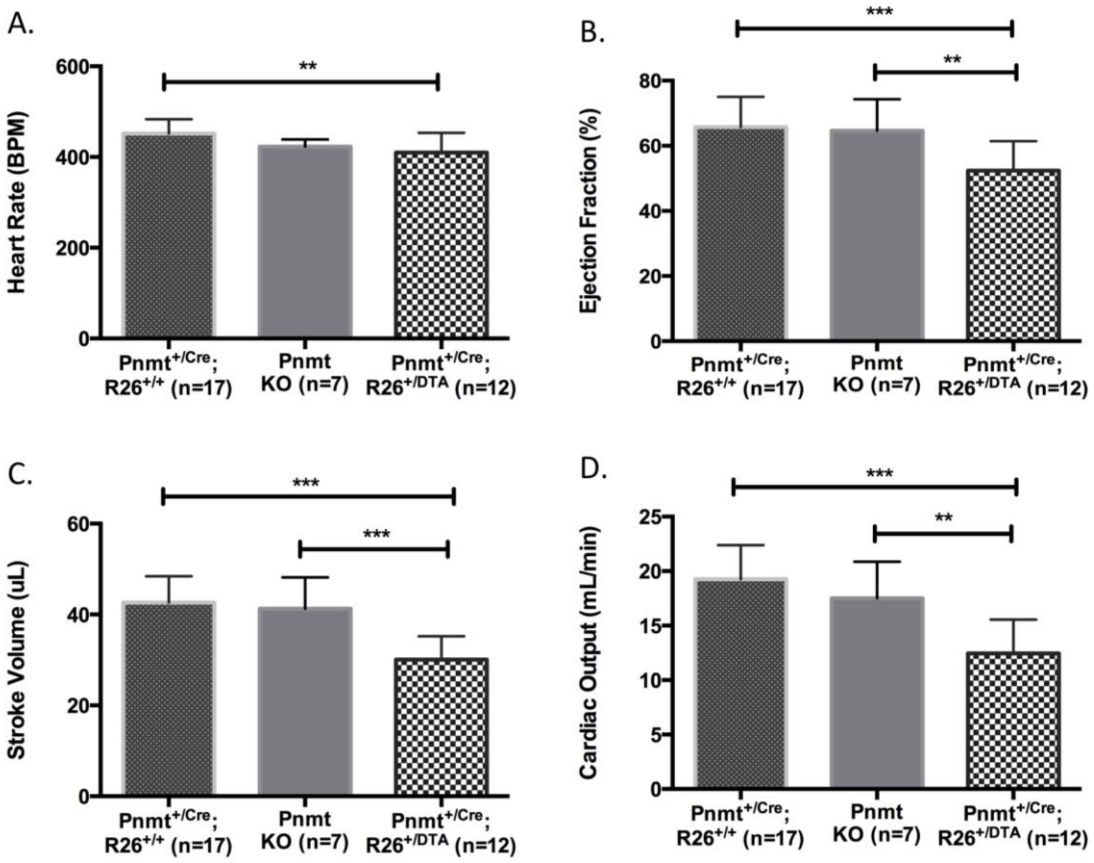

Figure 11: Pnmt$^{+/Cre}$: R26$^{+/DTA}$ mice have significantly reduced LV function compared to Pnmt KO mice at 5 months. Pnmt KO mice do not differ from Pnmt$^{+/Cre}$: R26$^{+/+}$. LV function was significantly lower in Pnmt$^{+/Cre}$; R26$^{+/DTA}$ compared to Pnmt KO and Pnmt$^{+/Cre}$; R26$^{+/+}$, but Pnmt KO did not differ from Pnmt$^{+/Cre}$; R26$^{+/+}$ for all parameters. (A) Heart rate. (B) Ejection fraction (C) Stroke volume (D) Cardiac output.

Table 4: Summary of Echocardiographic Analysis of Pnmt KO, Pnmt$^{+/Cre}$; R26$^{+/+}$, and Pnmt$^{+/Cre}$: R26$^{+/DTA}$ at 5 Months.
**0.05<p<0.01, ***0.01<p<0.001 from Pnmt+/Cre; R26+/+, ″ 0.05<p<0.01, ‴ 0.01<p<0.001 from Pnmt KO

	5 Month		
	Pnmt+/Cre; R26+/+	Pnmt +/Cre; R26+/DTA	Pnmt KO
	N=17	N=12	N=7
Heart Rate (BPM)	452 ± 8	410 ± 13″	423 ± 6
Stroke Volume (μL)	43 ± 1	30 ± 1***‴	41 ± 3
Ejection Fraction (%)	66 ± 2	52 ± 3***″	65 ± 4
Fractional Shortening (%)	36 ± 2	27 ± 2***″	35 ± 3
Cardiac Output (mL/min)	19 ± 1	12 ± 1***″	18 ± 1
Systolic Diameter (μm)	2.5 ± 0.1	2.7 ± 0.1	2.5 ± 0.1
Diastolic Diameter (μm)	3.9 ± 0.1	3.7 ± 0.1	3.8 ± 0.0

Pnmt$^{+/Cre}$; R26$^{+/DTA}$ Mice Recover Normal LV Function During Stress

To test whether Pnmt+ cells are involved in mediating the normal response to stress, we performed echocardiography in conscious, restrained mice. Restraint stress, or immobilization (IMO), mimics a mild stressor in mice, as they are prevented from performing the righting reflex. Surprisingly, Pnmt$^{+/Cre}$; R26$^{+/DTA}$ mice exhibited the same relative change in all parameters of left ventricular function from baseline to 1 hour IMO as the Pnmt$^{+/Cre}$; R26$^{+/+}$ controls. As shown in the M-modes in Figure 12, the LV is hypokinetic in Pnmt$^{+/Cre}$; R26$^{+/DTA}$ mice at baseline (top right). There is little movement of the left ventricular posterior wall (LVPW, white arrow) and the interventricular septum (IVS) exhibits little contraction during systole (red arrow). After one hour and two hours of immobilization, the LVPW and IVS exhibit faster, more forceful contractions.

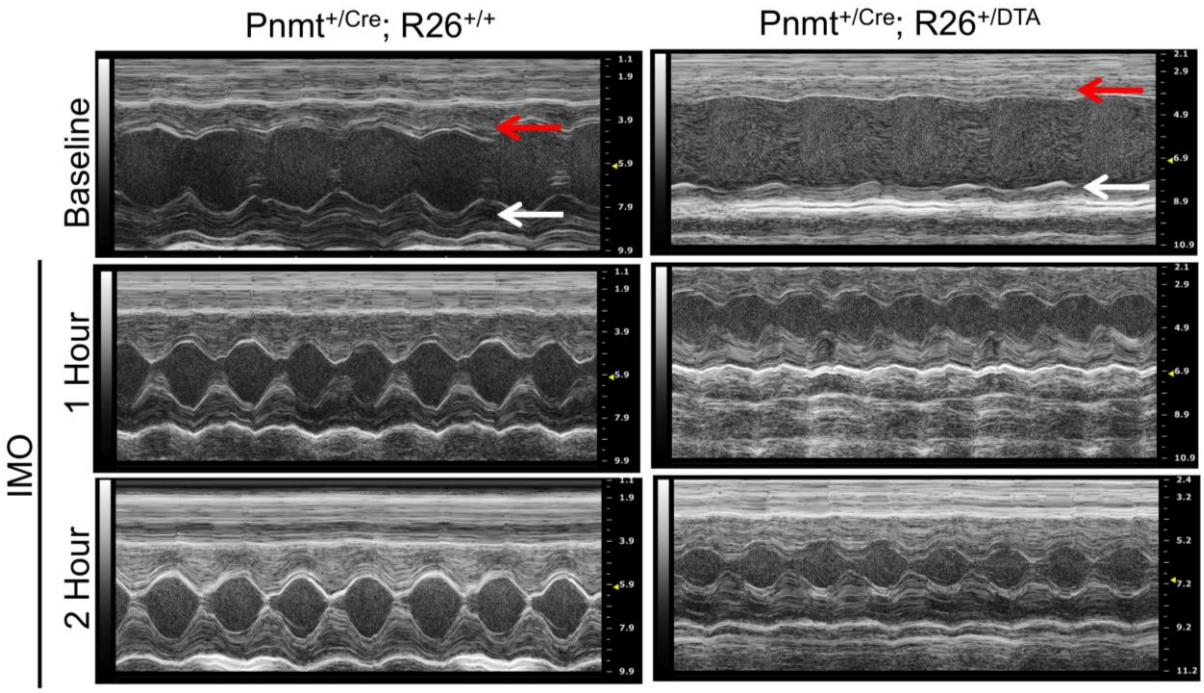

Figure 12: Representative M-Mode Images of the Left Ventricle Parasternal Long Axis during IMO $Pnmt^{+/Cre}$; $R26^{+/+}$ (left column) and $Pnmt^{+/Cre}$; $R26^{+/DTA}$ (right column) at Baseline (top row), and at One Hour (middle row) and Two Hours (bottom row) of Immobilization. Heart rate and contractility of the IVS (red arrow) and LVPW (white arrow) are hypokinetic at baseline, but increase substantially in response to stress in $Pnmt^{+/Cre}$; $R26^{+/+}$ controls and in $Pnmt^{+/Cre}$; $R26^{+/DTA}$ mice.

As shown in Figure 13, $Pnmt^{+/Cre}$; $R26^{+/DTA}$ mice exhibit the same general trend as $Pnmt^{+/Cre}$; $R26^{+/+}$ control mice during IMO. During stress, $Pnmt^{+/Cre}$; $R26^{+/DTA}$ mice responded with increased heart rate and increased ejection fraction, in a manner similar to controls. Stroke volume decreased due to the decrease in diastolic diameter during IMO and this lea to the decrease in cardiac output in both groups.

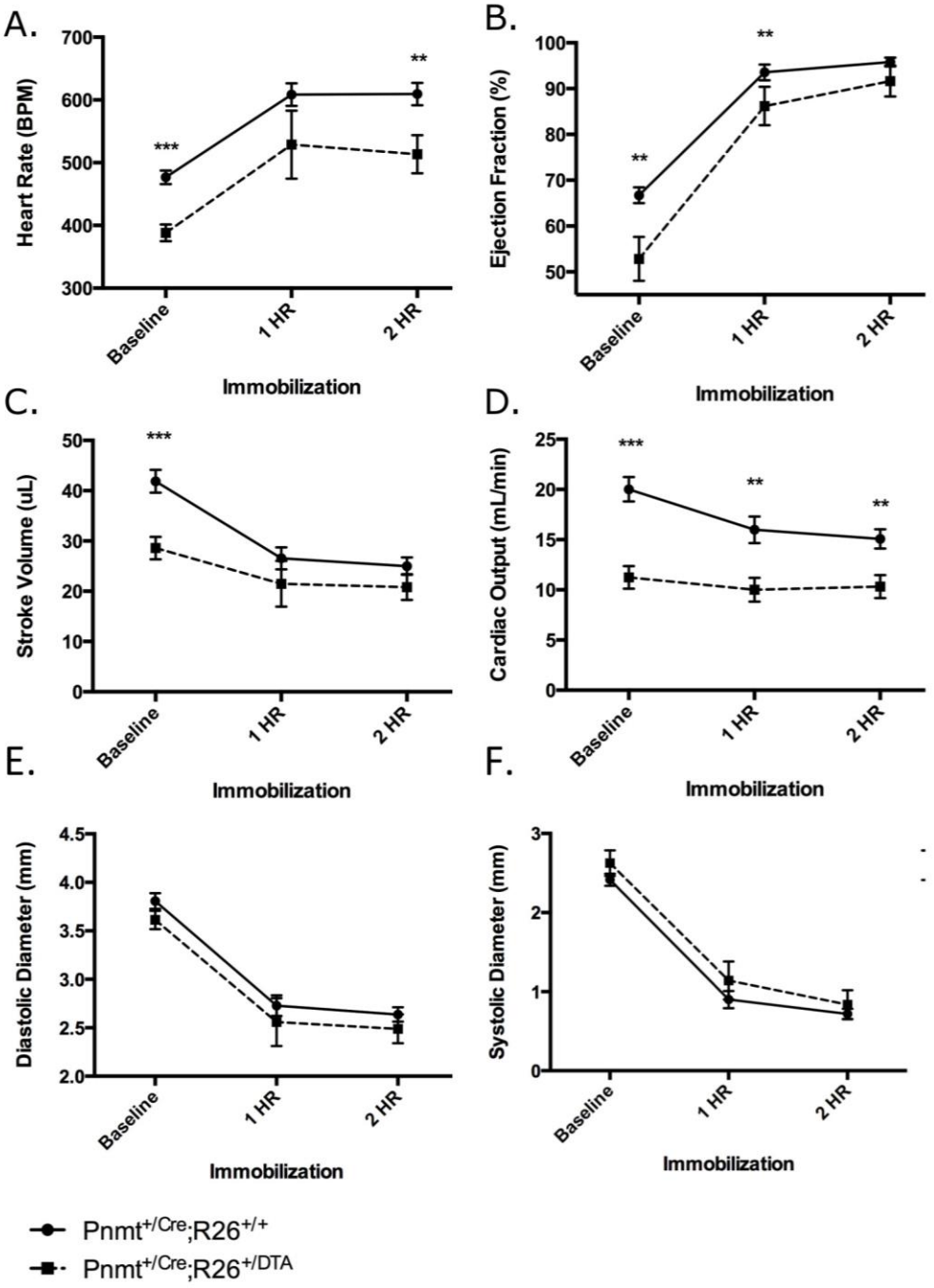

Figure 13: Pnmt$^{+/Cre}$; R26$^{+/DTA}$ Mice Display Normal Stress Response to Immobilization
Baseline, 1 Hour, and 2 Hour analysis of echocardiography. (A) Heart rate, (B) Ejection fraction, (C) Stroke volume, (D) Cardiac output, (E) Diastolic diameter, and (F) Systolic diameter.

Pnmt$^{+/Cre}$; R26$^{+/DTA}$ Mice Fail to Gain Weight into Adulthood

Pnmt$^{+/Cre}$; R26$^{+/DTA}$ mice appear normal at weaning compared to Pnmt$^{+/Cre}$; R26$^{+/+}$ littermate controls and R26$^{+/DTA}$ controls. By 4 months, Pnmt$^{+/Cre}$; R26$^{+/DTA}$ males have significantly reduced body mass, as shown in Figure 14, and by 5 months, females have significantly reduced body mass, as shown in Figure 15. Despite providing soft food on the floor of cages (Dietgel, Hydrogel, and moist food pellets), these mice fail to gain body mass and become emaciated. One male was found dead and one female was sacrificed due to emaciation at 3 months, and one male and one female were sacrificed due to emaciation at 5 months.

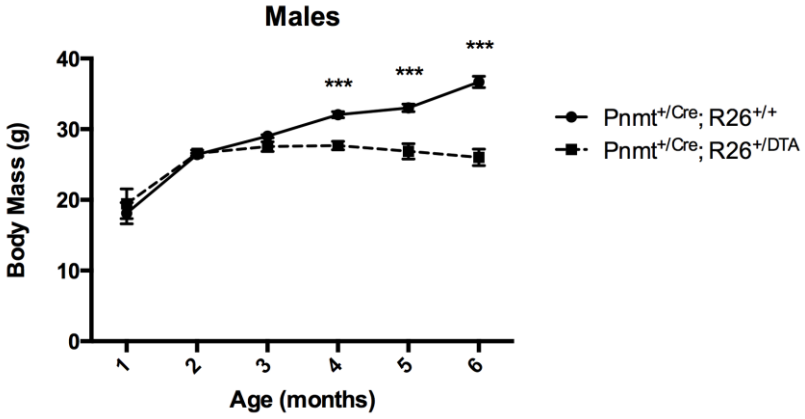

Figure 14: Lack of Weight Gain in Males

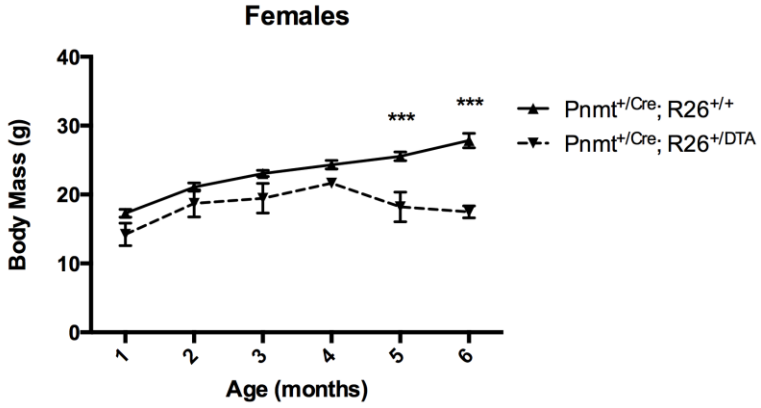

Figure 15: Lack of Weight Gain in Females

Pnmt$^{+/Cre}$; R26$^{+/DTA}$ Mice Exhibit Symptoms of Neurological Dysfunction

An unexpected result of this study was the development of clear neuromuscular dysfunction in these mice. Pnmt$^{+/Cre}$; R26$^{+/DTA}$ mice generally appeared normal at weaning (P21), but by 2-3 months of age, many began to exhibit hind limb clasping, altered gait, and kyphosis, indicators of neuromuscular dysfunction (Guyenet et al., 2010). By 5-6 months of age, 100% of Pnmt-Cre/DTA mice exhibit these phenotypes.

Figure 16A depicts the normal tail suspension reflex, in which both feet are held apart for the duration of the suspension test (approximately 10 seconds) and Figure 16B depicts the pathological leg splay, in which both legs clasp tightly upon immediately starting the test.

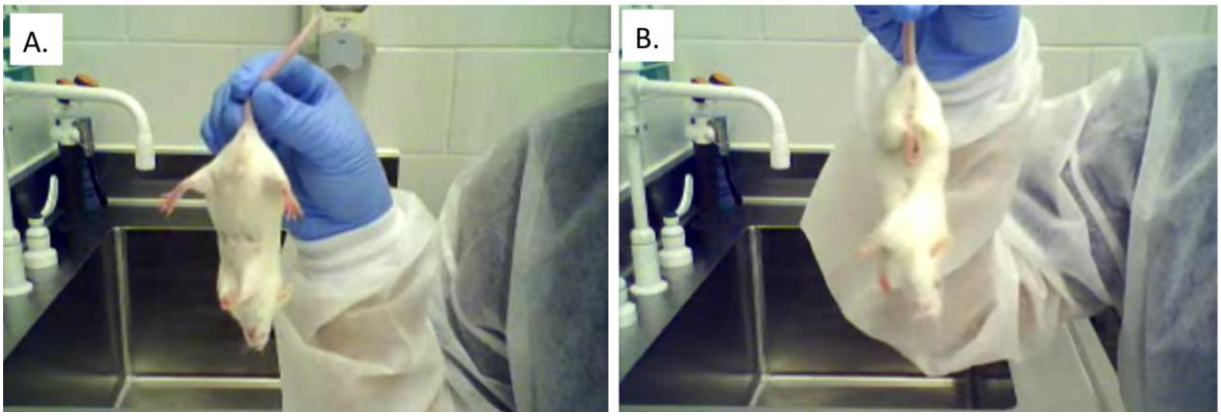

Figure 16: Hind Leg Clasping During Tail Suspension Reflex Test
(A) Pnmt$^{+/Cre}$; R26$^{+/+}$ controls exhibit normal tail suspension reflex, in which both legs are directed away from the abdomen. (B) Leg clasping in Pnmt$^{+/Cre}$: R26$^{+/DTA}$ mice.

The gait was clearly disturbed in these mice and they exhibited kyphosis, or hunched back. Kyphosis was present while walking and while standing still.

Grip strength was measured in 6-month-old adult mice. Grip strength of the forelimbs (Fig 17A) and in both limbs (Fig 17B) was significantly lower in Pnmt$^{+/Cre}$: R26$^{+/DTA}$ compared to Pnmt$^{+/Cre}$: R26$^{+/+}$.

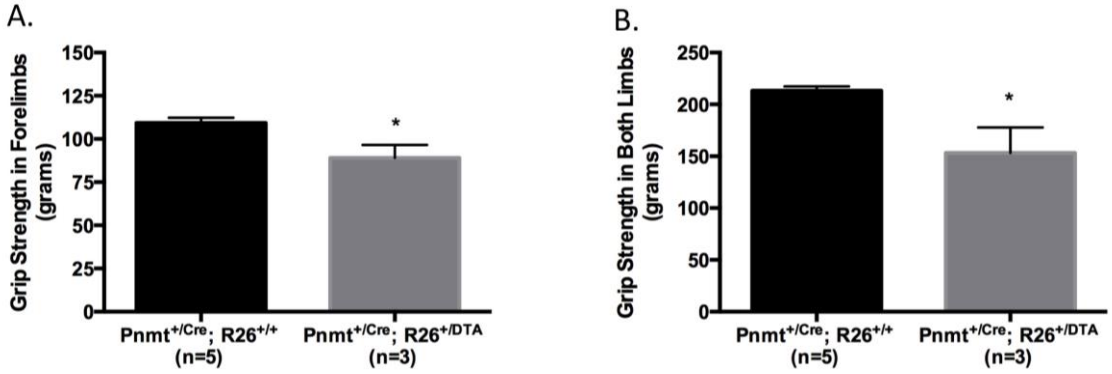

Figure 17: Decreased Grip Strength in Pnmt$^{+/Cre}$; R26$^{+/DTA}$ mice
(A) Forelimb grip strength is significantly lower in Pnmt$^{+/Cre}$; R26$^{+/DTA}$. (B) Grip strength of all limbs is significantly lower in Pnmt$^{+/Cre}$; R26$^{+/DTA}$.

DISCUSSION

Here, we showed for the first time that selective destruction of Pnmt+ cells results in significantly reduced cardiac function at rest, lack of normal weight gain, and neuromuscular dysfunction in $Pnmt^{+/Cre}$; $R26^{+/DTA}$ mice. Breeding $Pnmt^{Cre/Cre}$ mice with Rosa26-eGFP-DTA mice produced $Pnmt^{+/Cre}$; $R26^{+/DTA}$ mice that had significantly reduced Pnmt transcript, reduced Pnmt immunoreactive area in the adrenal glands, and adrenaline levels that are comparable to Pnmt knockout mice. $Pnmt^{+/Cre}$; $R26^{+/DTA}$ mice exhibited left ventricular dysfunction at rest, but Pnmt knockout mice did not. These results suggest that Pnmt+ cells are required for normal cardiovascular function, but adrenaline is not. Pnmt+ cell ablation also seems to disproportionally affect the number of females that survive to weaning, or 21 days. Further investigation is needed to assess these effects in females and whether this result is due to death in utero or during the early postnatal period.

Pnmt+ Cells of the Adult Heart

It has previously been shown that Pnmt+ cells contribute to development of the adult myocardium by becoming cardiomyocytes, intracardiac neurons, and intrinsic cardiac adrenergic cells (Ebert et al., 2004) (Osuala et al., 2011) (Slavikova et al., 2003) (Huang et al., 1996). Since adrenaline deficiency alone (in the Pnmt KO) does not recapitulate the phenotype of $Pnmt^{+/Cre}$; $R26^{+/DTA}$ mice, these cells likely contribute to basal cardiovascular function in a manner other than the secretion of adrenaline. In left ventricular myocardium, cardiomyocytes derived from Pnmt+ cells are likely being killed off and this may be the cause of the LV dysfunction. Histological examination of $Pnmt^{+/Cre}$; $R26^{+/DTA}$ hearts is expected to shed insight to the cause of the LV dysfunction.

Additionally, Pnmt immunoreactivity has been identified in the SA node of developing hearts (Ebert and Taylor, 2006). $Pnmt^{+/Cre}$; $R26^{+/DTA}$ mice exhibit bradycardia at rest, but Pnmt KO mice do not (Bao et al., 2007). Thus, Pnmt+ cells likely play a major role in establishing the rate of cardiac pacing, since this discrepancy cannot be attributed to adrenaline alone.

It is remarkable that $Pnmt^{+/Cre}$; $R26^{+/DTA}$ mice exhibited such robust response to immobilization stress. These mice, which had adrenaline levels close to knockout and had noradrenaline levels comparable to controls, responded to stress by increased heart rate and increased ejection fraction. These rapid responses to stress are likely mediated by the actions of noradrenaline at the Beta1 adrenergic receptor. The Beta1 adrenergic receptor is the major receptor responsible for increased heart rate in response to exercise-induced stress (Rohrer et al., 1999; Rohrer and Kobilka, 1998) (Chruscinski et al., 1999). Beta2 adrenergic receptor knockout mice display the normal exercise-induced tachycardia, but Beta1 adrenergic receptor knockout mice do not. The $Pnmt^{+/Cre}$; $R26^{+/DTA}$ mice exhibit bradycardia at rest, yet responded to stress with increased heart rate, but their heart rate was still significantly lower than controls during stress.

Furthermore, studies are currently underway to better distinguish the hormonal effects of adrenergic agonists in $Pnmt^{+/Cre}$; $R26^{+/DTA}$ mice. If the left ventricular dysfunction is due to loss of ventricular myocardium, and not from a lack of adrenergic receptor stimulation, then these mice should display the same phenotype in the presence of continuous agonism of adrenergic receptors at physiological levels. To test this hypothesis, we have begun a "rescue" experiment, where mice are given a modest level of nonselective beta and alpha adrenergic receptor agonist in the drinking water at weaning. (-)Isoproterenol is a nonselective beta adrenergic receptor agonist and L-phenylephrine is a nonselective alpha receptor agonist. Together, this concoction

of adrenergic receptor agonists rescues DBH knockout mice from heart failure (Thomas et al., 1998). DBH knockout mice lack adrenaline and noradrenaline and die of apparent heart failure in utero (Thomas et al., 1995). Infusion of (-) isoproterenol and L-phenylephrine can rescue DBH knockouts to term, suggesting that these drugs properly mimic the physiological actions of the absent hormones, noradrenaline and adrenaline. If the LV dysfunction is due to lack of sufficient adrenergic receptor stimulation, it is expected that the concoction of (-) isoproterenol and L-phenylephrine will not result in normal LV function.

Pnmt+ Cells Contribute to Neuromuscular Function

The severe neuromuscular dysfunction was unexpected in these mice. The current literature describing the role of Pnmt in locomotion is sparse. Studies using pharmacological inhibitors of Pnmt found decreased locomotor activity (Katz et al., 1978). Pnmt activity has been detected in cerebellum, at the same time that adrenaline levels begin to rise (Diaz Borges et al., 1980) (Diaz Borges and Chavez, 1980). Two forms of Pnmt mRNA have been detected in cerebellum (Andreassi et al., 1998). The effects of Pnmt knockout and adrenaline deficiency on neuromuscular function have not previously been published. Here, we report that the destruction of Pnmt+ cells results in severe ataxia, kyphosis, and hind limb clasping at an early age.

Thus far, no published reports indicate a role of Pnmt+ neurons or other Pnmt+ cell type in the maintenance of neuromuscular function. It is unlikely that adrenaline release from these cells is primarily responsible for their function, since Pnmt KO does not lead to any observable ataxia. It is possible that Pnmt is expressed transiently in certain subpopulations of cells that contribute to normal motor behavior, or that these neurons act primarily through some other neurotransmitter and express Pnmt at low levels. Others have suggested a role of adrenergic

neurons in modulating dopaminergic neurons of the extrapyramidal tract, but functional and anatomical evidence has been lacking (Katz et al., 1978). Our data warrant further investigation into the role of Pnmt+ cells in neural control of motor function.

Pnmt+ Cells in Appetite Control or Metabolism

$Pnmt^{+/Cre}$; $R26^{+/DTA}$ mice became severely emaciated at five to six months of age. Whether this severe lack of weight gain is secondary to heart failure or the result of altered feeding behavior or disturbed metabolic function has yet to be determined. Pnmt knockout mice do not have perturbed body mass or food intake, but do have decreased lean mass and increased body fat percentage (Sharara-Chami et al., 2010). Pnmt+ axons projecting from the brain stem to the paraventricular nucleus (PVN) of the hypothalamus have been identified (Rinaman, 2001). Additionally, electrolytic lesions to the PVN were shown to induce hyperphagia and obesity (Leibowitz et al., 1981) and noradrenaline injection directly to the PVN has been shown to stimulate preprandial drinking and feeding in satiated rats (Leibowitz, 1978). It is possible that Pnmt+ projections modulate PVN, reducing PVN activity, and leading to activation of appetite. Studies currently underway will help discern whether ablation of Pnmt+ cells reduces weight gain through dysregulation of appetite and feeding behavior or through metabolic dysregulation. Pnmt has also been identified in adipocytes, and their destruction cannot be ruled out as a mechanism of weight loss in these mice (Kvetnansky et al., 2012).

The results of this study support the literature reports of Pnmt expression in extra-adrenal tissue. The functional consequences of Pnmt+ cell ablation resulted in significantly diminished LV function, reduced weight gain, and severe symptoms of cerebellar ataxia. These symptoms were present in adolescence and progressively worsened into adulthood. The role of the cells that

mediate these effects is not likely through secretion of adrenaline, since the Pnmt knockout does not produce similar phenotypes. Overall, these results provide functional evidence for the role of Pnmt+ cells in normal cardiovascular function. Furthermore, Pnmt+ cells may also play a role in neuromuscular function and may be involved in appetite stimulation.

APPENDIX: PERMISSION FOR REPRINT OF FIGURE 2

JOHN WILEY AND SONS LICENSE
TERMS AND CONDITIONS

Mar 26, 2015

This Agreement between Aaron P Owji ("You") and John Wiley and Sons ("John Wiley and Sons") consists of your license details and the terms and conditions provided by John Wiley and Sons and Copyright Clearance Center.

License Number	3596161455012
License date	Mar 25, 2015
Licensed Content Publisher	John Wiley and Sons
Licensed Content Publication	Developmental Dynamics
Licensed Content Title	Targeted insertion of the Cre-recombinase gene at the phenylethanolamine n-methyltransferase locus: A new model for studying the developmental distribution of adrenergic cells
Licensed Content Author	Steven N. Ebert,Qi Rong,Steven Boe,Robert P. Thompson,Alexander Grinberg,Karl Pfeifer
Licensed Content Date	Oct 29, 2004
Pages	10
Type of use	Dissertation/Thesis
Requestor type	University/Academic
Format	Electronic
Portion	Figure/table
Number of figures/tables	1
Original Wiley figure/table number(s)	Figure 4
Will you be translating?	No
Title of your thesis / dissertation	GENETICALLY-PROGRAMMED SUICIDE OF ADRENERGIC CELLS IN THE MOUSE LEADS TO SEVERE LEFT VENTRICULAR DYSFUNCTION, IMPAIRED WEIGHT GRAIN, AND SYMPTOMS OF NEUROLOGICAL DYSFUNCTION
Expected completion date	May 2015
Expected size (number of pages)	65
Requestor Location	Aaron P Owji 1766 Seneca Blvd WINTER SPRINGS, FL 32708 United States Attn: Aaron P Owji

REFERENCES

Andreassi, J.L., 2nd, W.B. Eggleston, G. Fu, and J.K. Stewart. 1998. Phenylethanolamine N-methyltransferase mRNA in rat hypothalamus and cerebellum. *Brain research*. 779:289-291.

Bao, X., F. Liu, Y. Gu, C.M. Lu, and M.G. Ziegler. 2008. Impaired chronotropic response to exercise in mice lacking catecholamines in adrenergic cells. *Annals of the New York Academy of Sciences*. 1148:297-301.

Bao, X., C.M. Lu, F. Liu, Y. Gu, N.D. Dalton, B.Q. Zhu, E. Foster, J. Chen, J.S. Karliner, J. Ross, Jr., P.C. Simpson, and M.G. Ziegler. 2007. Epinephrine is required for normal cardiovascular responses to stress in the phenylethanolamine N-methyltransferase knockout mouse. *Circulation*. 116:1024-1031.

Chruscinski, A.J., D.K. Rohrer, E. Schauble, K.H. Desai, D. Bernstein, and B.K. Kobilka. 1999. Targeted disruption of the beta2 adrenergic receptor gene. *The Journal of biological chemistry*. 274:16694-16700.

Collier, R.J. 2001. Understanding the mode of action of diphtheria toxin: a perspective on progress during the 20th century. *Toxicon : official journal of the International Society on Toxinology*. 39:1793-1803.

Diaz Borges, J.M., and M. Chavez. 1980. Regional changes in adrenaline of rat brain during development. *Journal of neuroscience research*. 5:465-468.

Diaz Borges, J.M., L. Rodriguez, and M. Urbina. 1980. Regional changes in phenylethanolamine-N-methyltransferase of rat brain during development. *Journal of neuroscience research*. 5:363-367.

Ebert, S.N., J.M. Baden, L.H. Mathers, B.J. Siddall, and D.L. Wong. 1996. Expression of phenylethanolamine n-methyltransferase in the embryonic rat heart. *Journal of molecular and cellular cardiology*. 28:1653-1658.

Ebert, S.N., Q. Rong, S. Boe, and K. Pfeifer. 2008. Catecholamine-synthesizing cells in the embryonic mouse heart. *Annals of the New York Academy of Sciences*. 1148:317-324.

Ebert, S.N., Q. Rong, S. Boe, R.P. Thompson, A. Grinberg, and K. Pfeifer. 2004. Targeted insertion of the Cre-recombinase gene at the phenylethanolamine n-methyltransferase locus: a new model for studying the developmental distribution of adrenergic cells. *Developmental dynamics : an official publication of the American Association of Anatomists*. 231:849-858.

Ebert, S.N., and D.G. Taylor. 2006. Catecholamines and development of cardiac pacemaking: an intrinsically intimate relationship. *Cardiovascular research*. 72:364-374.

Ebert, S.N., and R.P. Thompson. 2001. Embryonic epinephrine synthesis in the rat heart before innervation: association with pacemaking and conduction tissue development. *Circ Res*. 88:117-124.

Evans, G.A. 1989. Dissecting mouse development with toxigenics. *Genes & development*. 3:259-263.

Guyenet, S.J., S.A. Furrer, V.M. Damian, T.D. Baughan, A.R. La Spada, and G.A. Garden. 2010. A simple composite phenotype scoring system for evaluating mouse models of cerebellar ataxia. *Journal of visualized experiments : JoVE*.

Huang, M.H., D.S. Friend, M.E. Sunday, K. Singh, K. Haley, K.F. Austen, R.A. Kelly, and T.W. Smith. 1996. An intrinsic adrenergic system in mammalian heart. *The Journal of clinical investigation*. 98:1298-1303.

Ivanova, A., M. Signore, N. Caro, N.D. Greene, A.J. Copp, and J.P. Martinez-Barbera. 2005. In vivo genetic ablation by Cre-mediated expression of diphtheria toxin fragment A. *Genesis (New York, N.Y. : 2000)*. 43:129-135.

Katz, R.J., B.B. Turner, K. Roth, and B.J. Carroll. 1978. Adrenergic control of motor activity: effects of PNMT inhibition upon open field behavior in the rat. *Pharmacology, biochemistry, and behavior*. 9:417-420.

Kvetnansky, R., J. Ukropec, M. Laukova, B. Manz, K. Pacak, and P. Vargovic. 2012. Stress stimulates production of catecholamines in rat adipocytes. *Cellular and molecular neurobiology*. 32:801-813.

Leibowitz, S.F. 1978. Adrenergic stimulation of the paraventricular nucleus and its effects on ingestive behavior as a function of drug dose and time of injection in the light-dark cycle. *Brain research bulletin*. 3:357-363.

Leibowitz, S.F., N.J. Hammer, and K. Chang. 1981. Hypothalamic paraventricular nucleus lesions produce overeating and obesity in the rat. *Physiology & behavior*. 27:1031-1040.

Moreira-Rodrigues, M., A.L. Graca, M. Ferreira, J. Afonso, P. Serrao, M. Morato, F. Ferreirinha, P. Correia-de-Sa, S.N. Ebert, and D. Moura. 2014. Attenuated aortic vasodilation and sympathetic prejunctional facilitation in epinephrine-deficient mice: selective impairment of beta2-adrenoceptor responses. *The Journal of pharmacology and experimental therapeutics*. 351:243-249.

Osuala, K., K. Telusma, S.M. Khan, S. Wu, M. Shah, C. Baker, S. Alam, I. Abukenda, A. Fuentes, H.B. Seifein, and S.N. Ebert. 2011. Distinctive left-sided distribution of adrenergic-derived cells in the adult mouse heart. *PloS one*. 6:e22811.

Quaife, C.J., G.W. Hoyle, G.J. Froelick, S.D. Findley, E.E. Baetge, R.R. Behringer, J.P. Hammang, R.L. Brinster, and R.D. Palmiter. 1994. Visualization and ablation of phenylethanolamine N-methyltransferase producing cells in transgenic mice. *Transgenic research*. 3:388-400.

Rinaman, L. 2001. Postnatal development of catecholamine inputs to the paraventricular nucleus of the hypothalamus in rats. *The Journal of comparative neurology*. 438:411-422.

Rohrer, D.K., A. Chruscinski, E.H. Schauble, D. Bernstein, and B.K. Kobilka. 1999. Cardiovascular and metabolic alterations in mice lacking both beta1- and beta2-adrenergic receptors. *The Journal of biological chemistry*. 274:16701-16708.

Rohrer, D.K., and B.K. Kobilka. 1998. Insights from in vivo modification of adrenergic receptor gene expression. *Annual review of pharmacology and toxicology*. 38:351-373.

Schmittgen, T.D., and K.J. Livak. 2008. Analyzing real-time PCR data by the comparative C(T) method. *Nature protocols*. 3:1101-1108.

Schneider, C.A., W.S. Rasband, and K.W. Eliceiri. 2012. NIH Image to ImageJ: 25 years of image analysis. *Nature methods*. 9:671-675.

Sharara-Chami, R.I., M. Joachim, M. Mulcahey, S. Ebert, and J.A. Majzoub. 2010. Effect of epinephrine deficiency on cold tolerance and on brown adipose tissue. *Molecular and cellular endocrinology*. 328:34-39.

Slavikova, J., J. Kuncova, J. Reischig, and M. Dvorakova. 2003. Catecholaminergic neurons in the rat intrinsic cardiac nervous system. *Neurochemical research*. 28:593-598.

Spatz, M., I. Nagatsu, C. Maruki, M. Yoshida, Y. Kondo, and J. Bembry. 1982. The presence of phenylethanolamine-N-methyltransferase in cerebral microvessel and endothelial cultures. *Brain research*. 240:191-194.

Thomas, S.A., B.T. Marck, R.D. Palmiter, and A.M. Matsumoto. 1998. Restoration of norepinephrine and reversal of phenotypes in mice lacking dopamine beta-hydroxylase. *Journal of neurochemistry*. 70:2468-2476.

Thomas, S.A., A.M. Matsumoto, and R.D. Palmiter. 1995. Noradrenaline is essential for mouse fetal development. *Nature*. 374:643-646.

Xia, J., N. Varudkar, C.N. Baker, I. Abukenda, C. Martinez, A. Natarajan, A. Grinberg, K. Pfeifer, and S.N. Ebert. 2013. Targeting of the enhanced green fluorescent protein reporter to adrenergic cells in mice. *Molecular biotechnology*. 54:350-360.

Ziegler, M.G., X. Bao, B.P. Kennedy, A. Joyner, and R. Enns. 2002. Location, development, control, and function of extraadrenal phenylethanolamine N-methyltransferase. *Annals of the New York Academy of Sciences*. 971:76-82.

Ziegler, M.G., B. Kennedy, and H. Elayan. 1989. Rat renal epinephrine synthesis. *The Journal of clinical investigation*. 84:1130-1133.